Research Square

Preprints are preliminary reports that have not undergone peer review.
They should not be considered conclusive, used to inform clinical practice,
or referenced by the media as validated information.

Aerial imaging sheets processed via X-ray lithography

Sho Amano

sho@laati.u-hyogo.ac.jp

University of Hyogo

Article

Keywords: aerial image, floating display, micromirror, X-ray lithography, flat optics, polymethylmethacrylate, DCRA

Posted Date: November 26th, 2026

DOI: https://doi.org/10.21203/rs.3.rs-11764830/v1

License: This work is licensed under a Creative Commons Attribution 4.0 International License.
Read Full License

Additional Declarations: No competing interests reported.

Abstract

We developed aerial imaging sheets (AIS) with microscale two-mirror arrays to produce aerial images using X-ray lithography. The dihedral angle (DA) of the two mirrors could be set at 90°, 0° or 105°. This enabled us to freely design the relative position of an object display and its aerial image. The sheets were very thin (0.2–1.5 mm) and lightweight, flat polymethylmethacrylate optics. We evaluated the brightness and resolution of the aerial images with image-processing software, and the results were consistent with the design specifications.

INTRODUCTION

Aerial imaging, which creates images that appear to float in midair, has a wide range of applications and has been actively investigated over the past two decades. During the COVID-19 pandemic, aerial displays attracted significant attention to prevent contagion in medical and food services, which required noncontact panel operation. Because of its ability to create a striking visual effect, aerial imaging is also expected to have applications in entertainment and digital signage.

In the field of aerial imaging, several types of micro-optical arrays that produce real images via geometric optics have been reported. These include reflective optics—such as dihedral-corner reflector arrays (DCRAs) [1, 2], roof-mirror grid arrays (RMGAs) [3, 4], crossed-mirror arrays (CMAs) [5], two-layer slit mirror arrays (2SMAs) [6], and retroreflective sheets (RRSs) [3, 7, 8]—and refractive optics such as gradient-index lens arrays [3, 9]. DCRAs, RMGAs, CMAs and 2SMAs produce aerial images using the same principle [1], in which twice-reflected rays from two micromirrors placed at a 90° dihedral angle (DA) produce a real image.

These remarkable features include no focal length and, theoretically, no distortion.

While this image is an “image” in terms of geometric optics, it is not being produced at the wavefront level. However, because the light rays are divided sufficiently finely, the human eye perceives it as an aerial image [10]. Because the two micromirrors need to reflect a part of the image geometrically optically, the DA does not have to be 90°.

Using the same principle, we developed a micro-optics array that we refer to as an “aerial imaging sheet (AIS)”, which consists of an “L-shaped” hole array, as shown in Fig. 1. This sheet has a simpler structure and is thinner than conventional optics. The holes work as two orthogonal mirrors needed for aerial imaging. Total reflection mirrors are created at the boundary between the sheet material and air, similar to a DCRA.

However, because the mirrors are inside the sheet, it is difficult to polish them in pre- or postprocesses. An AIS cannot be produced via conventional mechanical processes but can be produced via X-ray lithography. X-ray lithography can process devices at the micron scale with high precision and high aspect ratios, and in particular, the processed sidewalls become optical mirror faces with a surface

roughness of 30–50 nm [11]. In addition, X-ray lithography enables mass production (using the LIGA process [12]), and expected to result in low costs for future commercial products.

The two-mirror arrays of the DCRA, RMGA, CMA and 2SMA were limited to 90° DAs [Fig. 2(a)]. This limitation may be attributed either to the conditions required for retroreflection or mechanical fabrication constraints. With respect to the fixed DA, the relative position of an object display and its aerial image is determined in only one way, which may hinder the system design for aerial imaging. However, in principle, there is no reason that the DA must be a right angle. Thus, we developed AIS devices with various DAs via X-ray lithography. By varying the DA, we were able to freely design the positions of the aerial images with respect to a source display. For example, at a 0° DA, the two mirrors are parallel, and the aerial image appears parallel to an AIS-like microlens array [Fig. 2 (b)]. At a 105° DA, the aerial image appears on the same side as the AIS source display, similar to reflection [Fig. 2 (c)].

First, we developed an AIS with a DA of 90° [Fig. 2(a)] and investigated its aerial imaging characteristics. For this, we developed a new evaluation method for the brightness and resolution of aerial images by using image processing software. Last, we developed AISs with 0° and 105° DAs. In this paper, we discuss thin flat optics for aerial imaging of AISs processed by using X-ray lithography.

Methods

Microprocessing via X-ray lithography

X-ray lithography was performed at the BL-11 beamline [13] dedicated to microprocessing via deep X-ray lithography. This beamline is located in the “NewSUBARU” synchrotron radiation facility of the University of Hyogo. The stored electron energy was 1.5 GeV, and its maximum beam current was 400 mA. BL-11 propagates X-rays generated by a bending magnet to an end station through a toroidal mirror and two Be filters [Fig. 3(a)]. The mirror collimated the X-rays with horizontal and vertical divergence angles of 278 μrad and 14 μrad, respectively. The X-ray energy at the end station ranged from 2–7 keV. The X-ray mask consisted of a 10-μm thick gold layer on a polyimide membrane [Fig. 3(b)].

The gold layer had two orthogonal lines in an L-shaped hole array through which the X-rays passed (Fig. 4). Three masks (Mask 1, Mask 2, and Mask 3) were prepared with different hole dimensions, as shown in Table 1.

Table 1
Designed dimensions (see Fig. 4)

Mask 1	**l (μm)**	**w, g (μm)**
	150	**50**
Mask 2	200	50
Mask 3	355	50

Cast polymethylmethacrylate (PMMA) sheets (CLAREX; Nitto Jushi Kogyo, Tokyo) were used as the positive resist. PMMA is well suited for use as an X-ray resist for micro-optics because it has good optical quality and high optical transmittance. The X-ray resist in contact with each X-ray mask was placed on a four-axis motion stage. The stage can be tilted to change the X-ray incident angle (q), which was used when the DA was changed. During the exposure, the stage was scanned vertically for a uniform X-ray dose across the mask and the PMMA resist [Fig. 3(b)] because the beam had a narrow-arched pattern, and its intensity in the vertical direction had a Gaussian distribution [13]. The relationship between the X-ray dose and the processing depth is shown in Fig. 5. From this relationship, we determined the X-ray dose needed.

The PMMA samples developed immediately after exposure to avoid possible cracks [14]. A GG developer [15], which consisted of 60% 2-(2-butoxy-ethoxy) ethanol, 20% tetra-hydro-1,4-oxazine, 5% 2-aminoethanol-1, and 15% water by volume, was used. The temperature of the developer was kept constant at 38°C. The samples were placed face down in the developer, and stirring was used to release the dissolved particles. The samples were then rinsed in water and gently dried.

Measurements

The processed dimensions of the AIS were measured using a digital microscope (KEYENCE VHK-900), with an uncertainty of ± 0.4 μm. To produce aerial images, a liquid-crystal display (LCD) was used as the light source. The 7-inch LCD panel had 1920 × 1200 pixels with a pitch of 78.75 (W) μm × 78.75 (H) μm (FW279S, Zhangzhou SEETEC Optoelectronics Technology Co., Ltd., Fujian). Aerial images were captured with a 12-MP digital camera under constant operational conditions (ISO and shutter speed). We evaluated their brightness and resolution from the data in the captured images by using the image processing software “ImageJ” [16].

Results

Processed dimensions

First, three AISs with 90° DAs (normal type) were processed using the three masks. AIS1, AIS2, and AIS3 corresponded to AISs processed with Mask 1, Mask 2, and Mask 3, respectively. The thicknesses of the sheets were 300 μm, 400 μm, and 600 μm for Mask 1, Mask 2, and Mask 3, respectively, whose aspect ratios were 2, 2 and 1.7, respectively. The processed AISs are summarized in Table 2.

Table 2
Aerial imaging sheet (AIS) specifications

AIS1	**Mask**	**Thickness (μm)**	**Type (DA)**
	Mask 1	**300**	**Normal (90°)**
AIS2	Mask 2	400	Normal (90°)
AIS3	Mask 3	600	Normal (90°)
AIS4	Mask 1	200	Parallel (0°)
AIS5	Mask 2	1500	Reflection (60 + 45°)

The X-ray beam for AIS1, AIS2, and AIS3 was perpendicularly incident on the PMMA surface to create holes perpendicular to the surface. A constant 90° tilt angle of the stage was used during vertical scanning for this exposure. Thus, the stage surface was always vertical. X-ray lithography of the L-shaped hole array produced a microscale two-mirror array that extended completely through the PMMA sheets (Fig. 6). The entire processed area was a circle 3 cm in diameter.

Because the AIS produces images by converging optical rays reflected by each of the two mirrors, all the mirrors had to have the same angle (90° at the AISs) to the sheet surface to produce clear images. Although X-ray lithography results in precise microscale processing, determining the actual errors in the processed AISs was important. We examined the three AISs and measured the processed dimensions with an uncertainty of ± 0.4 μm. The measured results for AIS1, AIS2, and AIS3 exhibited the same pattern. Examples of the results for their front and rear surfaces are shown in Table 3, where Δ represents the difference between the front and rear surface dimensions. We found no significant differences ($\Delta < \pm 0.4$ μm) between the horizontal dimensions of the front and rear surfaces and only a slight difference ($\Delta > \pm 0.4$ μm) in the vertical dimensions, as shown in Table 3. This finding indicated the possibility of a slight taper structure in the vertical direction, and the maximum error for plumbness was 4 mrad.

Table 3
Examples of processed dimensions (see Fig. 6)

		l_v (μm)	w_v (μm)	l_h (μm)	w_h (μm)
	front	**152.4**	**49.8**	**151.8**	**48.4**
AIS1	rear	152.1	49.3	152.3	48.0
	Δ	0.3	0.5	0.5	0.4
	front	199.1	49.1	198.9	47.6
AIS2	rear	199.9	48.2	199.1	47.9
	Δ	0.8	0.9	0.2	0.3
	front	355.4	51.4	354.0	48.9
AIS3	rear	356.2	49.2	354.7	48.6
	Δ	0.8	2.2	0.7	0.3

Brightness and resolution

AIS1, AIS2, and AIS3 successfully produced aerial images. For example, an image from AIS2 when the LCD displayed the test character “A” is shown in Fig. 7(a). The LCD was placed 3 cm from the AIS surface at 45°. The AIS produced a real image of the LCD located on the opposite side of the AIS via the converging optical rays reflected by the two mirrors. The image position was plane symmetric with respect to the AIS surface, as indicated by the white acute angle in Fig. 7(a). The focus was set at this position, and the images were captured with a digital camera whose ISO and shutter speed were kept constant at 40 and 1/125 s, respectively.

When the mirror size increases and the aperture (see Fig. 6) becomes large, the aerial image becomes bright but blurred, and small differences are not detectable. In contrast, when the mirror size decreases and the aperture becomes small, the image becomes clear but dark, and small differences are detectable. In addition, diffraction effects cause darker and blurred images. Therefore, there is an optimized size for image brightness and resolution, which we investigated for AISs. We validated the design performance. Here, the distance between the AIS and the LCD was reduced to 3 cm to mitigate diffraction effects.

To evaluate the brightness, intensities integrated over the entire image in the captured data were calculated by using the software “ImageJ” and were normalized by the intensity of the LCD light. This parameter was used to represent “brightness”. The brightness values for AIS1, AIS2, and AIS3 are listed in Table 4. The brightness is proportional to the size of the two-mirror elements and the aperture ratio (AR). The AR can be represented [see Fig. 4] as

$$AR = \frac{l^2}{(l + w + g)^2}$$

1

.

The aspect ratio of the AIS must be greater than 2 to transmit an entire object image at a 45° angle of incidence. When the aspect ratio is less than 2, the transmitted light is decreased.

We denote the Fresnel loss of surfaces by L, which was measured to be 6%.

Therefore, the transmission of the AIS (T) can be represented as follows:

$$T = AR \times \frac{aspect\ ratio}{2} \times (1 - L)$$

2

.

As shown in Table 4, the brightness is in agreement with the calculated values of T.

Table 4
Brightness parameters of aerial images produced by an aerial imaging sheet (AIS)

AIS1	Measured Brightness	Calculated Transmittance
	0.38	**0.34**
AIS2	0.45	0.42
AIS3	0.49	0.49

The resolution of an aerial image was evaluated from the sharpness of the edge of the letter “A”, as shown in Fig. 8. The resolution of the image data was 28 μm, which was sufficiently small relative to the 78.75-μm LCD pixel size.

Changes in intensity with respect to the pixel position in each image produced by the original LCD, AIS1, AIS2, and AIS3 are shown in Fig. 9(a–d), respectively. The image resolution is also proportional to the mirror size. The theoretical limit (TL) of the resolution is a diagonal of each AIS element (see Fig. 8), and the TL can be represented as follows:

$$TL = \sqrt{2}(l + w + g)$$

3

.

The TLs calculated by Eq. (3) are inserted in Fig. 9(a–d). The measured results were consistent with these limits.

The AISs exhibited good performance as designed for aerial imaging, and X-ray lithography was successful.

Demonstration of parallel and reflection types

We developed new types of AISs by changing the DA. When the DA was 0° and the two mirrors were parallel, the aerial image floated parallel to the AIS similar to a microlens array, creating the “parallel type” AIS [Fig. 2(b)]. When the DA was 105°, the aerial image floated on the same side as the source display for the AIS like a reflection, creating the “reflection type” AIS [Fig. 2(c)]. To process parallel and reflection-type AISs, the same L-shaped pattern masks were used. Although L-shaped hole arrays, which consist of microscale two-mirror arrays, were also produced in the PMMA sheets, only one mirror “A” of the two was used in these scenarios (Fig. 9). Optical rays travel parallel to the surfaces “B” and “B” do not function as mirrors.

With respect to the parallel type, the tilt angle q of the stage in Fig. 3(b) was kept constant at 45°, and the stage was vertically scanned during the X-ray exposure. After this process, parallel through-holes of mirrors were oriented at a 45° angle relative to the sheet surface [Fig. 9(a)]. AIS4 was processed using Mask1 and a PMMA sheet with a thickness of 200 μm (Table 2). With respect to the reflection type, a second step at a constant − 60° was added after the above process. V-shaped mirror holes were created in the sheet [Fig. 9(b)]. AIS5 was processed using Mask2 and a PMMA sheet with a thickness of 1500 μm (Table 2). During each test, the LCD was placed parallel to the AIS surface. In Fig. 7(b), real images of the LCD were produced on the opposite side of AIS4 with respect to the LCD and on the same side of AIS5 in Fig. 7(c). Thus, we demonstrated how AIS4 and AIS5 aerial images are produced by these new types of AISs.

Discussion

The brightness and resolution of the aerial images were consistent with the design specifications, indicating that the processed holes have good mirror faces with no significant scattering losses. The evaluation method we developed using “ImageJ” software proved useful. We detected slight errors in the processed dimensions for the vertical direction; however, these did not greatly affect the performance. The X-ray beam was sufficiently collimated, and these errors were likely caused by sagging of the mask polyimide [17] because the errors were only in the vertical direction; thus, we will improve the processing accuracy by replacing the polyimide with a carbon substrate [18]. X-ray lithography enabled us to process normal AISs as well as parallel and reflection AISs. We also presented their aerial images. An aerial image can be obtained even if a DA is not a right angle that produces retroreflection. The AISs enabled us to freely design the relative position of an object display and its aerial image. The AISs were very thin (0.2–1.5 mm) and very light (< 0.2 g/cm^2) because the specific gravity of the PMMA was 1.19 [19].

Conclusion

By using X-ray lithography, we developed new AIS optics for aerial images.

We also developed a new evaluation method for the brightness and resolution of aerial images by using “ImageJ” software.

Compared with those of conventional optics, the features of an AIS we invented are summarized as follows.

- It is a thin flat optic with a simple structure.
- Changing the DA increases the flexibility of the system design for aerial imaging.
- The simple structure of the AIS reduced the production cost. The LIGA process can enable mass production, with low costs for future commercial products.

An AIS of novel flat optics can be processed via X-ray lithography and can increase the range of applications.

Declarations

Competing interests

The authors declare that they have no conflicts of interest.

Funding

Research Assistant Funding Program of the Kagaku-Gijutu-Kouen-Zaidan of Hyogo University (2024).

Author Contribution

S. A: Conceptualization, methodology, data analysis, writing—original draft preparation, writing—review and editing, software, validation, visualization. The author contributed to all aspects of the research.

Data Availability

Data underlying the results presented in this paper are not publicly available at this time but may be obtained from the authors upon reasonable request.

References

1. Maekawa, S., Nitta, K. & Matoba, O. Transmissive optical imaging device with micromirror array. *Proc. SPIE*6392, 63920E (2006).
2. Miyazaki, D. et al. Floating volumetric image formation using a dihedral corner reflector array device. *Appl. Opt.* **52**, A281 (2013).
3. Maekawa, S., Nitta, K. & Matoba, O. Advanced in passive image elements with micromirror. *Proc. SPIE*6803, 68030B (2008).
4. Miyazaki, D., Hirano, N., Maeda, Y., Ohno, K. & Maekawa, S. Volumetric display using a roof mirror grid array. *Proc. SPIE* 7524, 75240N (2010).
5. Yamamoto, H., Kujime, R., Bando, H. & Suyama, S. Aerial LED signage by use of crossed-mirror array. *Proc. SPIE*8643, 864302 (2013).
6. Principles and Mechanismas of Aerial Display (Aerial Imaging Technology) ASKA3D. https://aska3d.com/ja/technology.html?lang=en
7. Yamamoto, H. & Suyama, S. and Aerial 3D LED display by use of retroreflective sheeting. *Proc. SPIE*8648, 86480Q (2013).
8. Yamamoto, H., Tomiyama, Y. & Suyama, S. Floating aerial LED signage based on aerial imaging by retro-reflection (AIRR). *Opt. Express*. **22**, 26919 (2014).
9. Arai, J., Okano, F., Hoshino, H. & Yuyama, I. Gradient-index lens-array method based on real-time integral photography for three-dimensional images. *Appl. Opt.* **37**, 2034–2045 (1998).
10. Maeda, Y. Air floating display by a dihedral corner reflector array. *ITEJ (The J. Inst. image Inform. Telev. engineers)*. **75**, 194–197 (2021). (in Japanese).
11. Rogner, A., Eicher, J., Munchmeyer, D., Peters, R-P. & Mohr, J. The LIGA technique – what are the new opportunities? *J. Michromech Microeng*. **2**, 133–140 (1992).
12. Saile, V., Wallrabe, U., tabata, O. & Korvink, J. G. (eds) *LIGA and Its Application* (Wiley-VCH Verlag GmbH & Co. KGaA, 2009).
13. Takeuchi, M., Yamaguchi, A. & Utsumi, Y. Deep X-ray lithography system with a uniform and high-accuracy fabrication area established in beamline BL11 at NewSUBARU. *J. Synchrotron Rad*. **26**, 528–534 (2019).
14. Watanabe, T. et al. Study of Dihedral-Corner-Reflector-Array fabrication process using soft X-ray deep X-ray lithography. *J. Photopolym. Sci. Technol.* **36**, 97–100 (2023).
15. Glashauser, W. & Ghica, G. V. Method of stress-free development of irradiated polymethylmethacrylate. *German Patent* **4**,393,129 (1983). GG developer is the name of an organic developer.
16. ImageJ, I. Processing and Analysis in Java. https://imagej.net/ij/
17. Achenbach, S. et al. Structure quality in deep X-ray lithography applying commercial polyimide-bases masks. *Microsyst. Technol.* **13**, 349–353 (2007).
18. Yamaguchi, A., Maekawa, S., Yamane, T., Okada, I. & Utsumi, Y. Fabrication of a dihedral corner reflector array for a floating image manufactured by X-ray lithography using synchrotron radiation.

Trans. JIEP (The Japan Inst. Electron. Packing). **8**, 23–28 (2015).
19. CLAREX General Properties. https://clarex.co.jp/en/products/data/

Figures

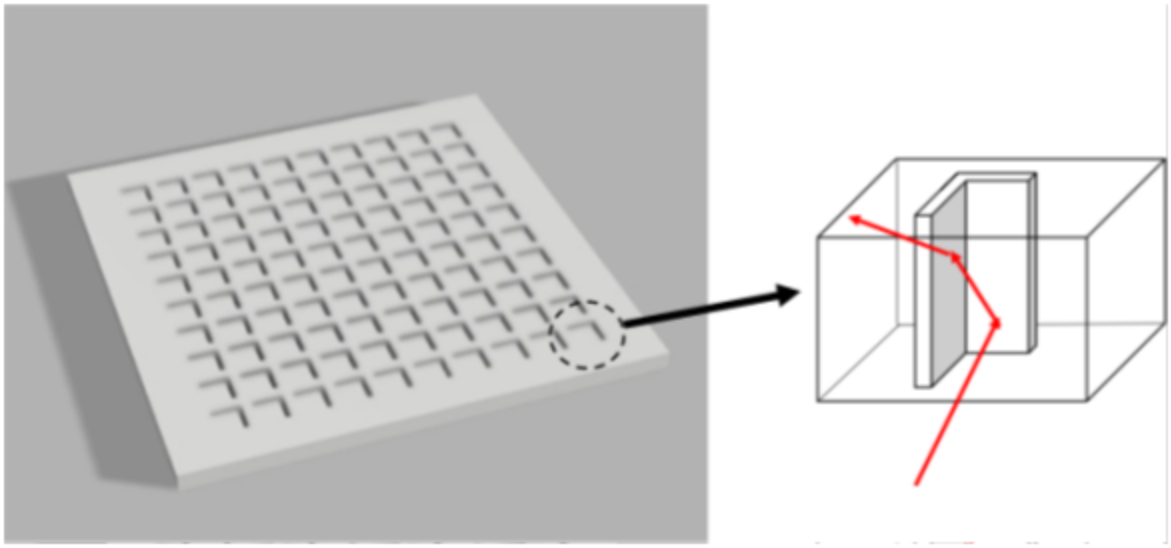


Figure 1

Schematic of an aerial imaging sheet (AIS).

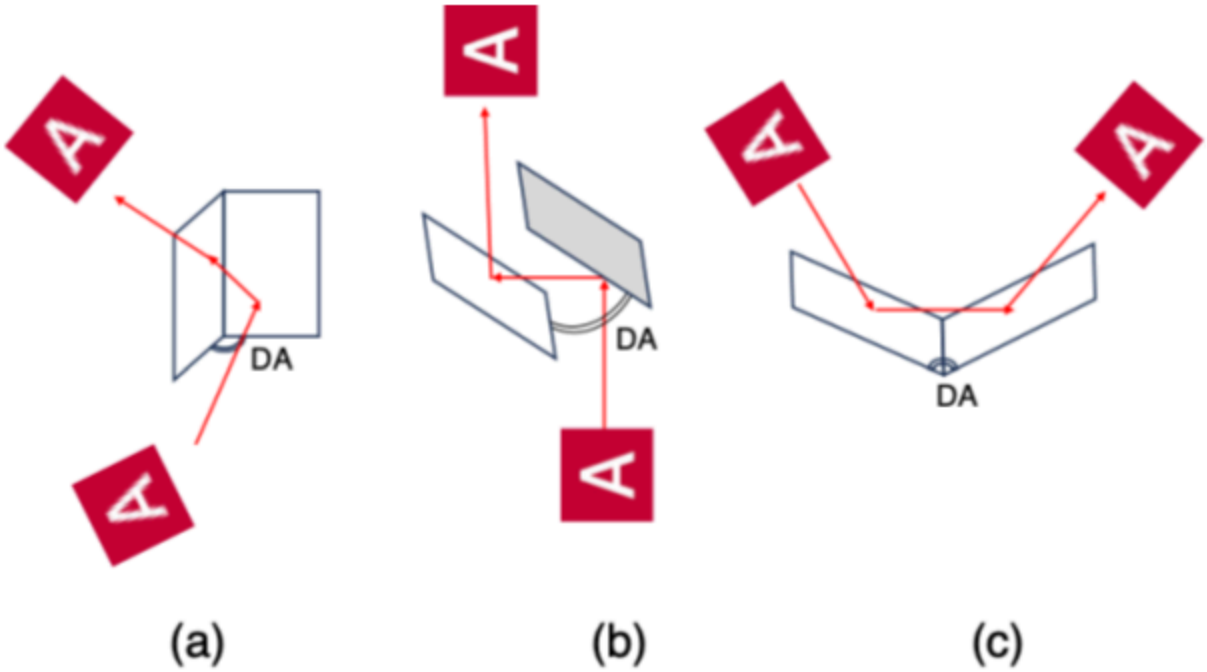


Figure 2

Trajectories of twice-reflected optical rays by a microscale mirror pair where the dihedral angle (DA) is (a) 90°, (b) 0°, and (c) 105°.

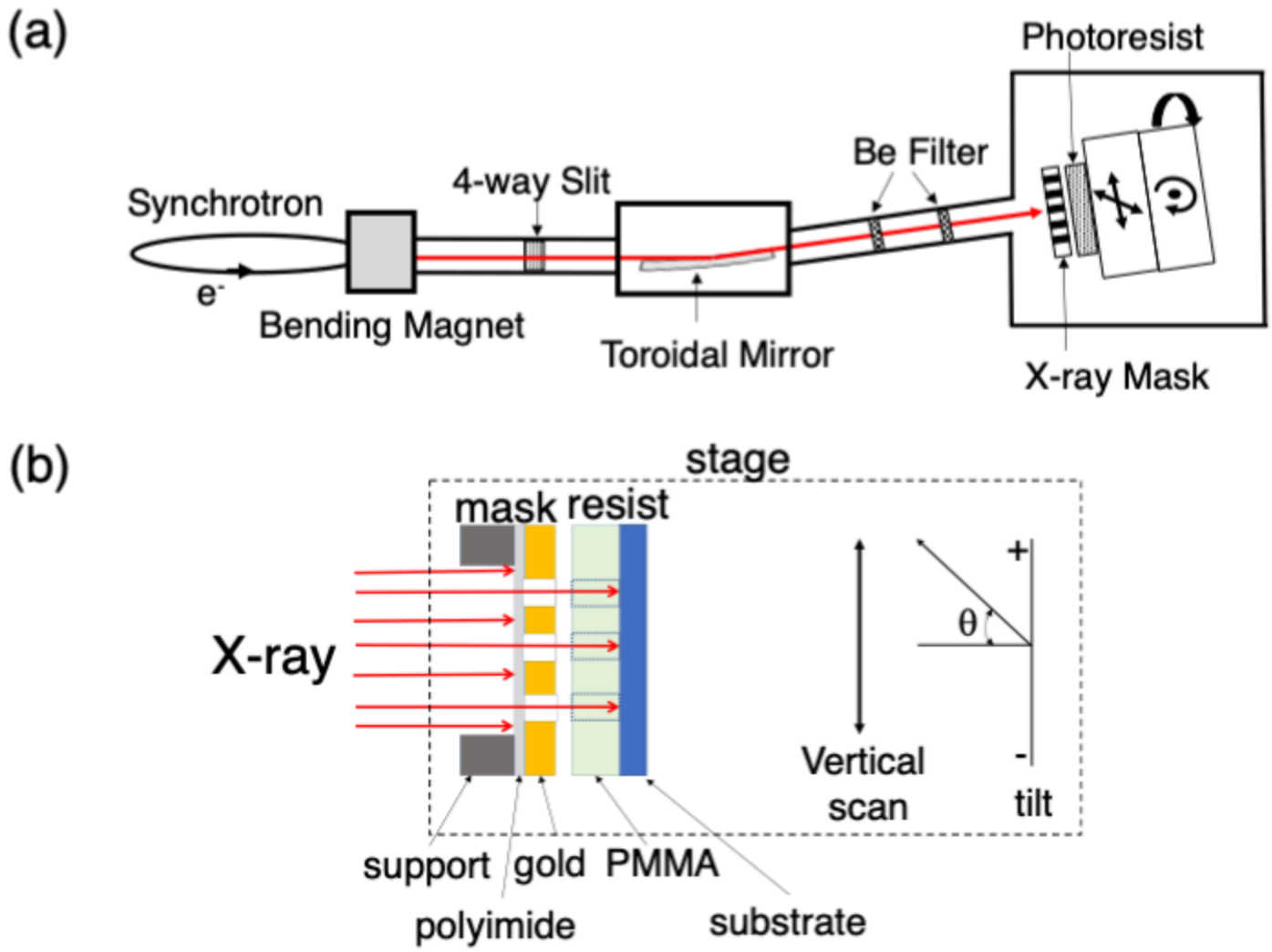


Figure 3

Schematic of (a) the BL11 deep X-ray lithography beamline at the NewSUBARU facility and (b) the mask and resist on the motion stage.

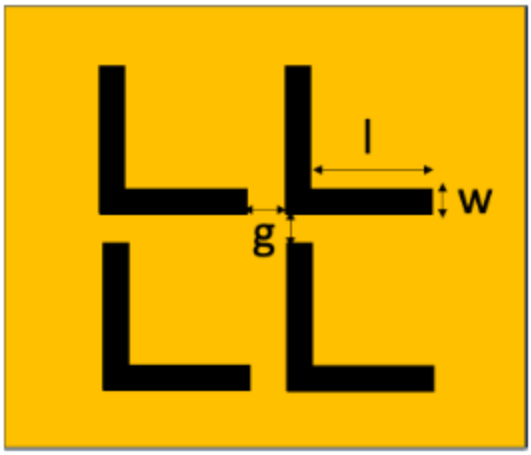


Figure 4

L-shaped hole pattern in the gold layer of the X-ray mask.

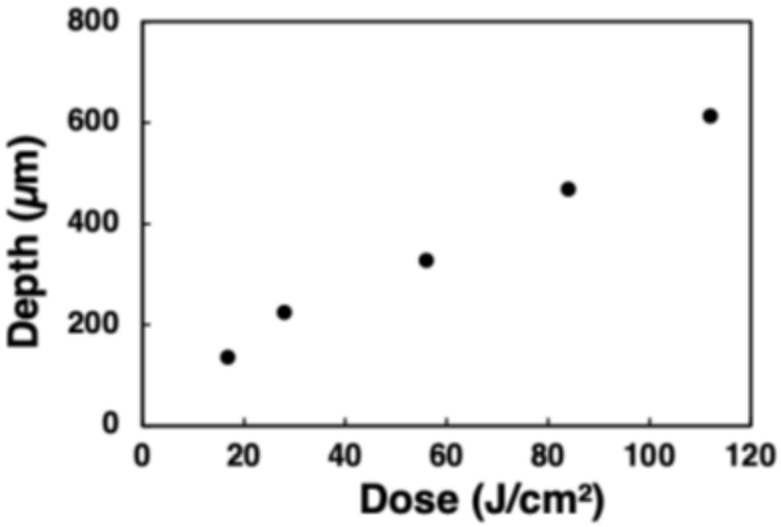


Figure 5

Dependence of the processing depth of polymethylmethacrylate (PMMA) sheets on the X-ray dose.

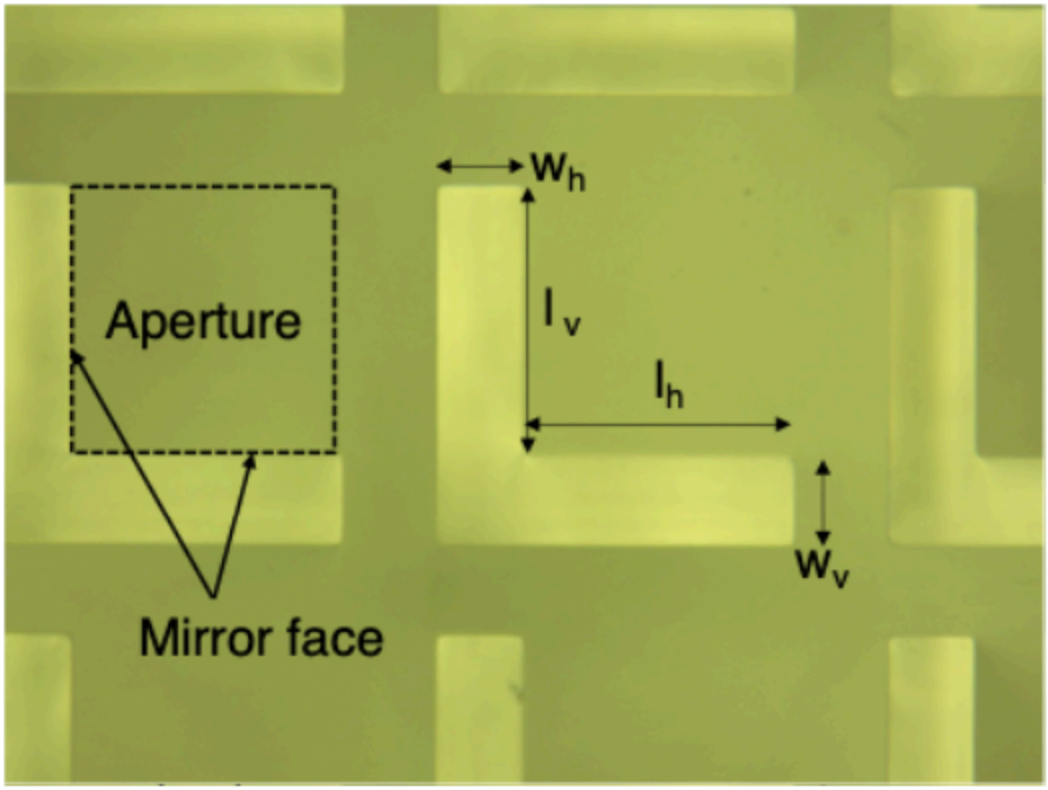


Figure 6

Photograph of AIS1 with L-shaped through holes (AIS represents aerial imaging sheet). Light enters through rear apertures, reflects off mirrors twice, and exits through front apertures.

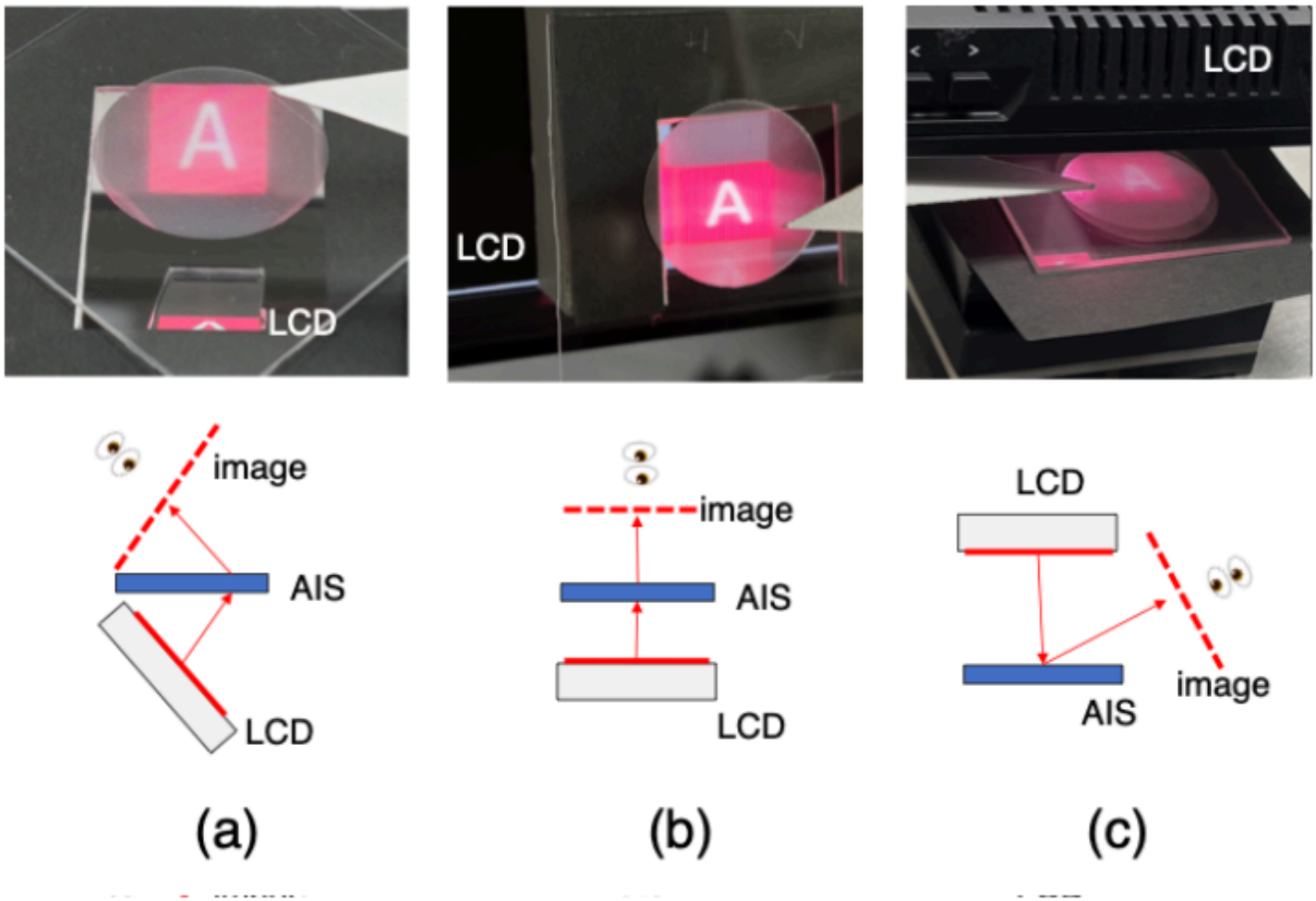


Figure 7

(upper) Photograph of the aerial image produced by (a) AIS2 (normal type, dihedral angle (DA) = 90°), (b) AIS4 (parallel type, DA = 0°), and (c) AIS5 (reflection type, DA = 105°). White acute angles indicate focus positions, and AIS represents aerial imaging sheet. (lower) Setup to observe the aerial image.

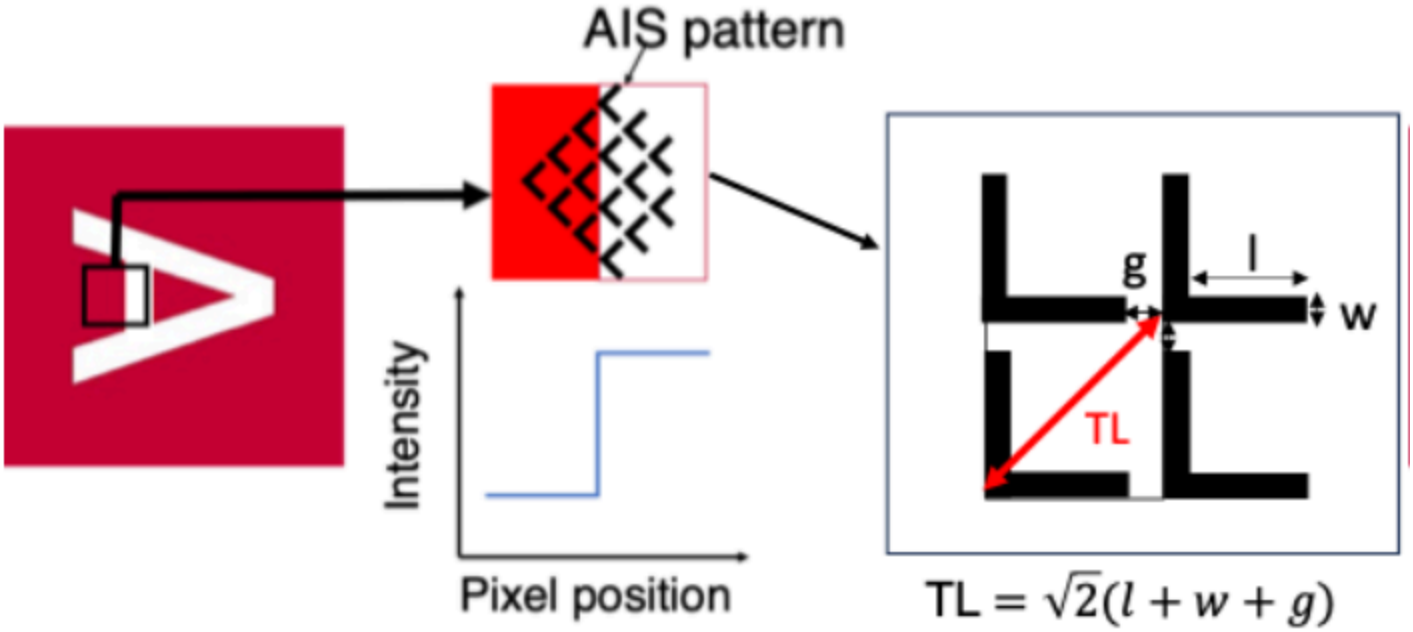


Figure 8

Evaluated area for the plots of image intensity versus pixel position and explanation of the TL (theoretical limit).

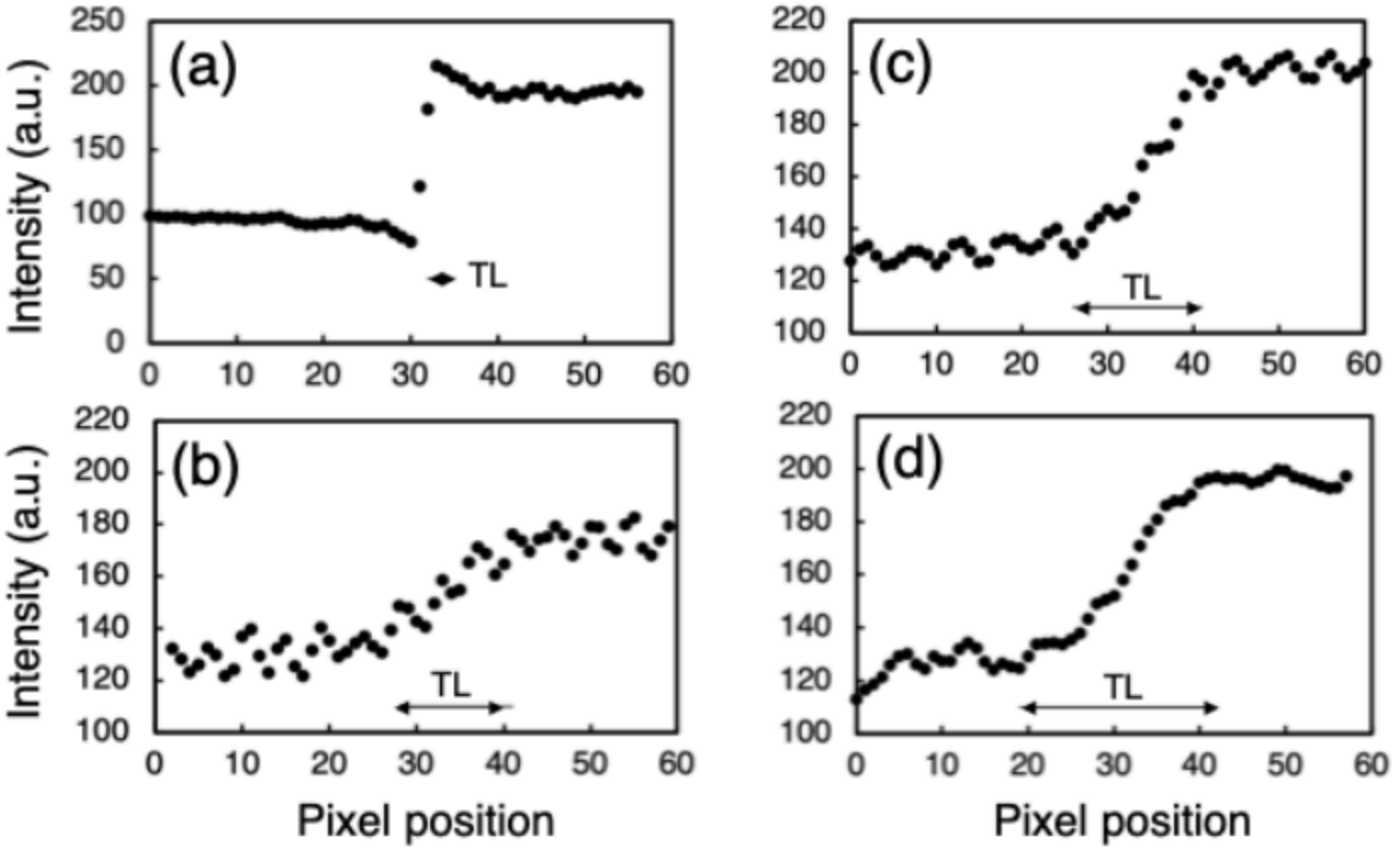


Figure 9

Image intensity versus pixel position. Measured results (a) for the objective image of the liquid crystal display (LCD), (b) for the aerial images produced by AIS1, (c) AIS2, and (d) AIS3. TL represents theoretical limit, and AIS denotes aerial imaging sheet.

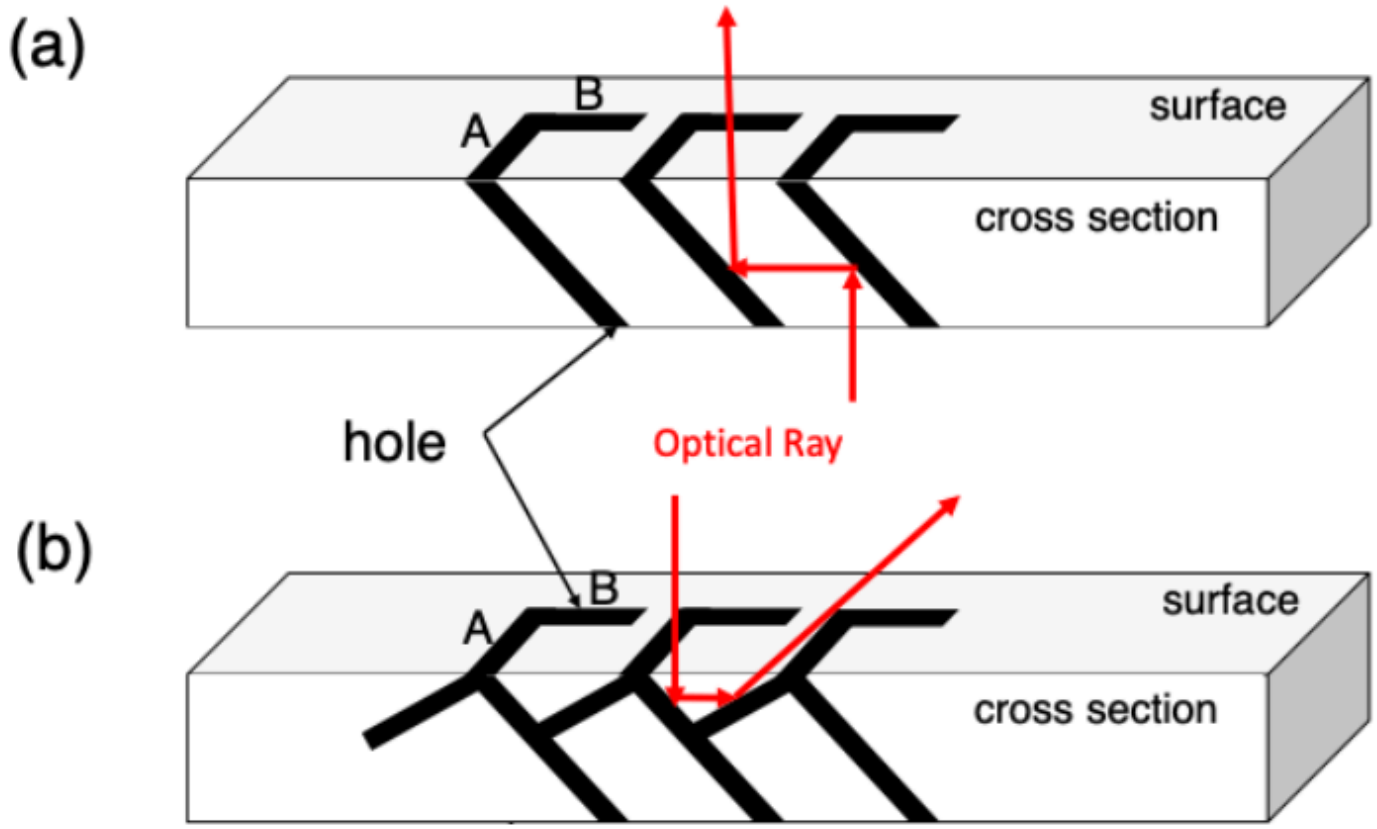


Figure 10

Processed holes shown in the cross-section of the sheet after X-ray exposure with tilt angles of (a) 45°, and (b) 45° and −60°. Only “A” holes were used as mirrors, whereas “B” holes were not used.